Acta Crystallographica Section D
Biological Crystallography
ISSN 0907-4449

Structure of the UNC5H2 death domain

Noriko Handa,[a] Mutsuko Kukimoto-Niino,[a] Ryogo Akasaka,[a] Kazutaka Murayama,[a,b] Takaho Terada,[a] Makoto Inoue,[a] Takashi Yabuki,[a] Masaaki Aoki,[a] Eiko Seki,[a] Takayoshi Matsuda,[a] Emi Nunokawa,[a] Akiko Tanaka,[a] Yoshihide Hayashizaki,[a] Takanori Kigawa,[a,c] Mikako Shirouzu[a] and Shigeyuki Yokoyama[a,d]*

[a]RIKEN Genomic Sciences Center, Tsurumi, Yokohama 230-0045, Japan, [b]Tohoku University Biomedical Engineering Research Organization, Aoba, Sendai 980-8575, Japan, [c]Department of Computational Intelligence and Systems Science, Interdisciplinary Graduate School of Science and Engineering, Tokyo Institute of Technology, 4259 Nagatsuta-cho, Midori-ku, Yokohama 226-8502, Japan, and [d]Department of Biophysics and Biochemistry, Graduate School of Science, The University of Tokyo, Bunkyo-ku, Tokyo 113-0033, Japan

Correspondence e-mail: yokoyama@biochem.s.u-tokyo.ac.jp

Received 20 July 2006
Accepted 26 September 2006

PDB Reference: UNC5H2 death domain, 1wmg, r1wmgsf.

UNC5Hs (UNC5H1–4) are netrin 1 receptors that are involved in axonal guidance and neuronal migration. They are dependence receptors that mediate apoptosis in the absence of netrin 1. UNC5H2-induced apoptosis depends on the interaction of the death domain at the C-terminus with the DAP-kinase death domain and caspase cleavage near the transmembrane region. Here, the crystal structure of the mouse UNC5H2 death domain has been determined at 2.1 Å resolution. The domain adopts a six-helix bundle fold, which is similar to those of the other members of the death-domain superfamily. The UNC5H2 death domain is a dimer in the crystal and in solution. This homodimerized structure may represent the structure of the death domain when netrin 1 binds to the UNC5H2 receptor. Homodimerization of UNC5H2 may block the access of caspase to the cleavage site. In the death-domain dimer, residues in $\alpha3$ and the 3_{10}-helix preceding $\alpha3$ and the residues in $\alpha4$ make significant contacts, mainly by hydrophobic and van der Waals interactions.

1. Introduction

Netrin 1 is a secreted protein that guides migrating cells and axons to their targets in the developing nervous system. It acts through the netrin 1 receptors of the deleted in colorectal cancer (DCC) protein and UNC5H (Keino-Masu *et al.*, 1996; Leonardo *et al.*, 1997; Mehlen & Mazelin, 2003). The UNC5H receptors, UNC5H1–4 in vertebrates, are single-pass transmembrane receptors. Their intracellular regions contain a death domain (DD) at their carboxy-termini (Hofmann & Tschopp, 1995). The DCC family receptors, DCC and neogenin in vertebrates, are also single-pass transmembrane receptors. Results obtained with *Xenopus* assays suggested that axon attraction to netrin 1 involves DCC expression in the absence of UNC5H, while axon repulsion involves the simultaneous expression of UNC5H and DCC (Hong *et al.*, 1999; Fig. 1*a*). The evidence obtained from *Drosophila melanogaster* suggests that UNC5H homologues can also elicit repulsion to netrin 1 in the absence of DCC (Keleman & Dickson, 2001) (Fig. 1*a*).

UNC5H1–3 and DCC are also known as dependence receptors. Such receptors create cellular states of dependence on their ligands (Bredesen *et al.*, 2004; Mehlen & Furne, 2005). In the absence of netrin 1, UNC5H1–3 and DCC induce apoptosis, while the function of UNC5H4 has not been well characterized (Llambi *et al.*, 2001; Mehlen *et al.*, 1998; Bredesen *et al.*, 2004; Mehlen & Furne, 2005; Fig. 1*b*). UNC5H1–3 and DCC are cleaved by caspase and this cleavage is required for the apoptotic induction of UNC5H2 and DCC (Llambi *et al.*, 2001; Arakawa, 2004; Mehlen *et al.*, 1998). The

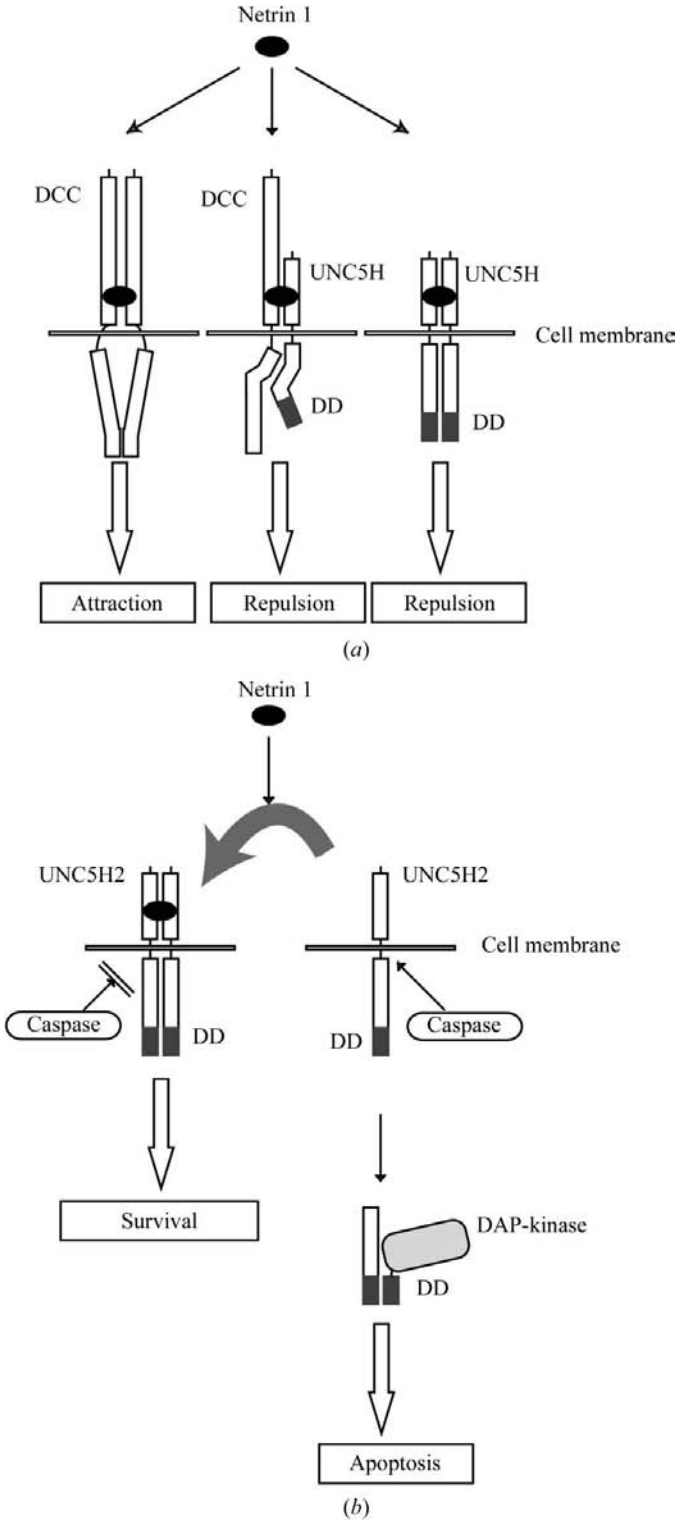

Figure 1
Netrin 1 and its receptors, UNC5H and DCC. (*a*) Netrin 1 binding to both DCC and UNC5H or UNC5H alone induces axon repulsion, whereas netrin 1 binding to DCC alone induces axon attraction. (*b*) A model of the signalling pathways from UNC5H2 and netrin 1. In the absence of netrin 1, UNC5H2 is cleaved by caspase at the cleavage site in the intracellular region. The released segment interacts with DAP-kinase in part through the respective death domains of UNC5H2 and DAP-kinase, which induce apoptosis. In the presence of netrin 1, UNC5H2 may homodimerize stably, thus blocking caspase cleavage.

UNC5H2 death domain, located at the C-terminus of the caspase cleavage site, is essential for apoptosis (Llambi *et al.*, 2001). It was recently shown that UNC5H2 interacts with the serine/threonine kinase death-associated protein kinase (DAP-kinase; Llambi *et al.*, 2005). This interaction is mediated in part through the respective death domains of UNC5H2 and DAP-kinase and induces the UNC5H2 pro-apoptotic activity (Llambi *et al.*, 2005; Fig. 1*b*). Therefore, it is possible that netrin 1 binding to UNC5H2 induces the homodimerization of UNC5H2, thus blocking caspase cleavage (Arakawa, 2005; Fig. 1*b*).

UNC5H1–3 are also thought to be tumour suppressors, because their expression is down-regulated in various cancers (Thiebault *et al.*, 2003). In a mouse model, inhibition of UNC5H-induced and DCC-induced apoptosis by enforced expression of netrin 1 in the gastrointestinal tract was shown to lead to tumour progression (Mazelin *et al.*, 2004).

The death domain is present in many proteins in apoptotic signalling pathways and in a variety of other proteins with various functions (Feinstein *et al.*, 1995). The death domain is involved in protein–protein interactions and forms homodimers and heterodimers. A total of four death-domain (DD) solution structures, the Fas DD (Huang *et al.*, 1996), the p75 neurotrophin DD (Liepinsh *et al.*, 1997), the FADD DD (Jeong *et al.*, 1999; Berglund *et al.*, 2000; Carrington *et al.*, 2006) and the TNFR-1 DD (Sukits *et al.*, 2001), have been reported. Three death-domain crystal structures, the Tube DD in complex with the Pelle DD (Xiao *et al.*, 1999), the IRAK-4 DD (Lasker *et al.*, 2005) and the RAIDD DD (Park & Wu, 2006), have also been reported. The death domains have been divided into two subtypes. The Fas, FADD, TNFR-1, Tube and Pelle DDs belong to subtype 1 and the p75 neurotrophin DD belongs to subtype 2 (Feinstein *et al.*, 1995). The amino-acid sequence of the UNC5H2 DD is most similar to that of the p75 neurotrophin DD. The death domains have a six-helix bundle fold arranged in an antiparallel manner. This fold is also characteristic of death-effector domains (DED), caspase-recruitment domains (CARD) and PYRIN domains. The death, DED, CARD and PYRIN domains comprise the death-domain superfamily (Weber & Vincenz, 2001, Kohl & Grutter, 2004).

In the present study, we solved the crystal structure of the mouse UNC5H2 death domain. The formation of a death-domain dimer was confirmed by analytical ultracentrifugation. This homodimeric structure may be induced by netrin 1 binding to the UNC5H2 receptor *in vivo*.

2. Materials and methods

2.1. Cloning, protein expression, purification and crystallization

The mouse UNC5H2 cDNA clone is from the FANTOM RIKEN full-length cDNA clone collection (FANTOM clone ID 6330415E02; Carninci *et al.*, 2003). The UNC5H2 DD (854–943) was produced as a 136-amino-acid protein with an N-terminal histidine-affinity tag and a tobacco etch virus

(TEV) protease-cleavage site. The selenomethionine (SeMet) substituted protein was synthesized by the *Escherichia coli* cell-free system using the dialysis method (Kigawa *et al.*, 2004; Wada *et al.*, 2003; Kigawa, Yabuki & Yokoyama, 1999; Kigawa, Yabuki, Yoshida *et al.*, 1999). The internal solution (27 ml) was dialyzed in three dialysis tubes (Spectra/Por 7, MWCO 15 000, Spectrum) against the external solution (270 ml) at 303 K for 4 h with shaking. After dialysis, the internal solution was centrifuged at 16 000*g* at 277 K for 20 min. The supernatant was loaded onto a HiTrap Chelating (GE Healthcare Biosciences) column (5 ml) previously equilibrated with 20 m*M* Tris–HCl buffer pH 8.0 containing 1 *M* NaCl and 15 m*M* imidazole and was eluted with 20 m*M* Tris–HCl buffer pH 8.0 containing 500 m*M* NaCl and 500 m*M* imidazole. The sample buffer was exchanged to 20 m*M* Tris–HCl buffer pH 8.0 containing 1 *M* NaCl and 15 m*M* imidazole with a HiPrep 26/10 desalting column. The histidine-affinity tag was cleaved using 100 µl TEV protease (4 mg ml^{-1}) at 303 K for 1 h. The reaction solution was loaded onto a HiTrap Chelating column (5 ml) and was eluted as described previously. The protein sample was desalted on a HiPrep 26/10 desalting column and was eluted with 20 m*M* Tris–HCl buffer pH 8.0 containing 2 m*M* DTT. Next, the protein sample was loaded on a HiTrap Q (GE Healthcare Biosciences) column (1 ml) previously equilibrated with 20 m*M* Tris–HCl buffer pH 8.0 containing 2 m*M* DTT and was eluted with a linear gradient of 0–1.0 *M* NaCl in 20 m*M* Tris–HCl buffer pH 8.0 with 2 m*M* DTT. Finally, the protein sample was loaded onto a HiLoad 16/60 Superdex 75 (GE Healthcare Biosciences) column previously equilibrated with 20 m*M* Tris–HCl buffer pH 8.0 containing 150 m*M* NaCl and 2 m*M* DTT and was eluted with this buffer. The native protein prepared for the analytical ultracentrifugation experiments was synthesized and purified in the same way as the SeMet-substituted protein.

Table 1
Data-collection and refinement statistics.

Values in parentheses are for the highest resolution shell.

Data set	Remote	Peak	Edge
Data collection and processing			
Wavelength (Å)	0.96400	0.979006	0.979363
Resolution range (Å)	50–2.1	50–2.1	50–2.1
Measured reflections	128687	128108	125864
Unique reflections	35889	35775	35704
Redundancy	3.6	3.6	3.5
Completeness (%)	99.6 (99.2)	99.4 (97.4)	99.2 (96.6)
R_{sym}† (%)	6.9 (24.1)	8.2 (25.6)	6.3 (23.8)
$I/\sigma(I)$	13.0 (4.1)	11.3 (3.2)	13.7 (4.9)
Phasing statistics			
Resolution range (Å)	20–2.1		
Se sites per monomer	3		
FOM_{MAD}‡	0.35		
Model refinement			
Resolution range (Å)	40–2.1		
No. of reflections	65800		
No. of protein atoms	4070		
No. of SO_3 molecules	7		
No. of SO_4 molecules	3		
No. of water molecules	185		
R_{work}/R_{free}§ (%)	22.9/26.9		
Average *B* factor (Å^2)	45.2		
Stereochemistry			
R.m.s.d. for bond length (Å)	0.007		
R.m.s.d. for bond angles (°)	1.20		
Residues in the Ramachandran plot			
Most favoured region (%)	88.4		
Additional allowed regions (%)	11.6		
Modelled residue ranges			
Monomer *A*	854–943		
Monomer *B*	855–914, 919–941		
Monomer *C*	854–916, 918–942		
Monomer *D*	854–914, 918–942		
Monomer *E*	854–941		
Monomer *F*	855–941		

† $R_{sym} = (\sum_h \sum_i |I_{hi} - \langle I_h \rangle| / \sum_h \sum_i |I_{hi}|)$, where *h* indicates unique reflection indices and *i* indicates symmetry-equivalent indices. ‡ Figure of merit after *SOLVE* phasing. § $R_{work} = \sum |F_{obs} - F_{calc}| / \sum F_{obs}$ for all reflections and R_{free} was calculated using randomly selected reflections (5%).

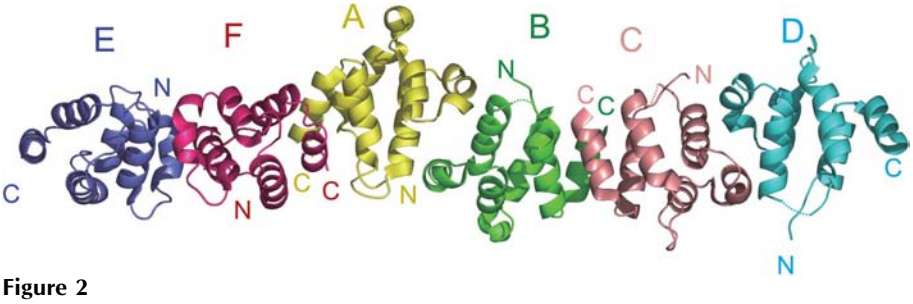

Figure 2
Interfaces between the UNC5H2 DDs. The six death domains of the crystallographic asymmetric unit are coloured differently. The disordered regions are represented by dotted lines. This figure was drawn using *PyMOL* (http://www.pymol.org).

2.2. Data collection and processing

Data for the multiwavelength anomalous dispersion (MAD) method were collected at three different wavelengths at BL26B1 of SPring-8, Harima, Japan (Table 1). All data were processed using the *HKL*-2000 and *SCALEPACK* programs (Otwinowski & Minor, 1997). The positions of the Se atoms and the initial MAD phases were determined using the program *SOLVE* (Terwilliger & Berendzen, 1999) and the MAD phases were improved with *RESOLVE* (Terwilliger, 2004). The resulting electron-density map was clear.

Crystals of the SeMet-substituted protein were grown at 285 K by the sitting-drop vapour-diffusion method (protein at 5.0 mg ml^{-1}) against a reservoir solution containing 100 m*M* MES pH 6.5 and 1.8 *M* $MgSO_4$. The crystals belong to space group *C*2, with unit-cell parameters a = 124.88, b = 47.21, c = 121.18 Å, β = 119.56°. There are six monomers in the asymmetric unit.

2.3. Model building and structural refinement

The data collected at the high remote wavelength (0.9640 Å) were used to refine the model. The *RESOLVE* program (Terwilliger, 2004) was used to build 452 residues without side chains

automatically. The remaining 70 residues and side chains were built with the program *TURBO-FRODO* and multiple cycles of model building and refinement were performed.

The model was refined using *CNS* v.1.1 (Brünger *et al.*, 1998). There are six monomers in the asymmetric unit. The final model has good geometry, as examined by *PROCHECK* (Laskowski *et al.*, 1996): 88.4% of the residues have φ/ψ angles in the most favoured region of the Ramachandran plot and 100% are in the allowed regions. The data-collection and refinement statistics and modelled residue ranges are listed in Table 1.

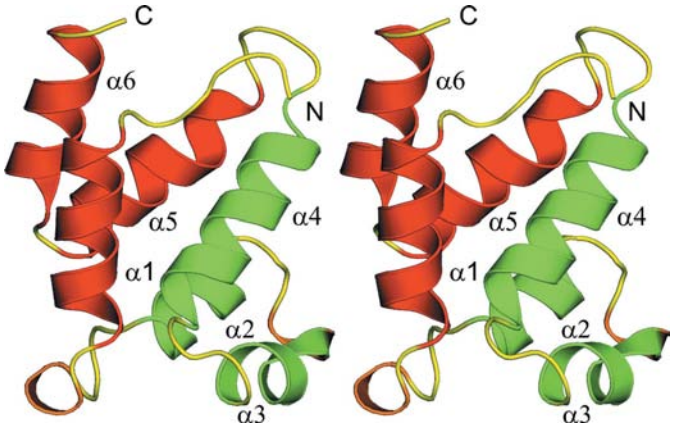

Figure 3
Ribbon diagram of the UNC5H2 DD monomeric structure (stereoview). The $\alpha1$, $\alpha5$ and $\alpha6$ helices are red, the $\alpha2$, $\alpha3$ and $\alpha4$ helices are green, the 3_{10}-helices are orange and the random coils are yellow. This figure was drawn using *MOLSCRIPT* (Kraulis, 1991) and *RASTER3D* (Merritt & Murphy, 1994).

2.4. Analytical ultracentrifugation

All analytical ultracentrifugation experiments were carried out with a Beckman Optima XL-I analytical ultracentrifuge. The sample buffer was 20 m*M* Tris–HCl pH 8.0, 150 m*M* NaCl and 5 m*M* β-mercaptoethanol and all experiments were performed at 293 K. The solvent density and protein partial specific volume ($\overline{\upsilon}$) were estimated with *SEDNTERP* (Laue *et al.*, 1992). Sedimentation-velocity data were obtained at 40 000 rev min^{-1} using an Epon two-channel centrepiece, with loading concentrations of 0.36, 0.25 and 0.16 mg ml^{-1} native protein. The data were analyzed with the program *SEDFIT* (Schuck, 1998). Sedimentation-equilibrium experiments were carried out with six-channel centrepieces, with loading concentrations of 0.36 and 0.18 mg ml^{-1}. Data were obtained at 18 000, 22 000 and 26 000 rev min^{-1}. A total equilibration time of 16 h was used for each speed, with scans taken at 12 and 14 h to ensure that equilibrium had been reached. The absorbance wavelength was 280 nm and the optical baseline was determined by overspeeding at 35 000 rev min^{-1} at the end of data collection. The equilibrium data were fitted using the manufacturer's software.

3. Results

3.1. Overall structure

The six monomers *A*, *B*, *C*, *D*, *E* and *F* of the UNC5H2 DD in the asymmetric unit (Fig. 2) superimpose on one another with a root-mean-square deviation (r.m.s.d.) of 0.52–1.92 Å for the 73 C$^{\alpha}$ atoms of residues 858–912 and 921–938 as calculated using *MOLMOL* (Koradi *et al.*, 1996). These crystal structures

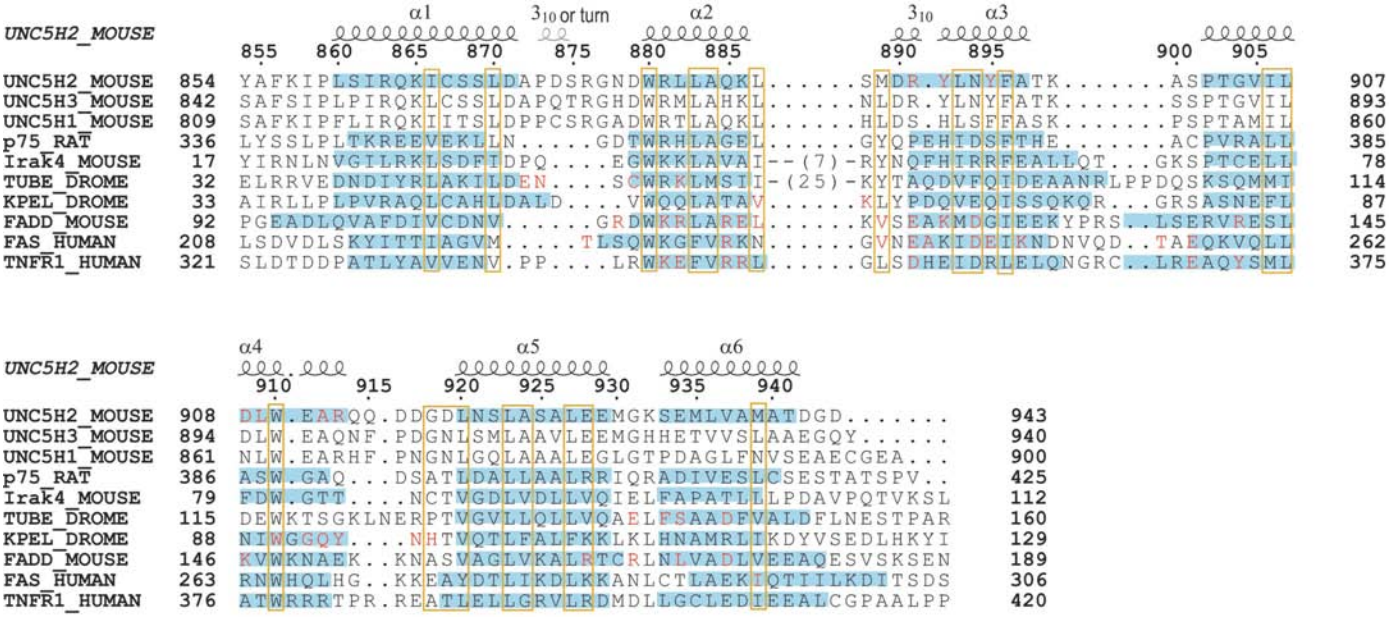

Figure 4
Structure-based sequence alignment of death domains. The first column shows the protein identifier. Helices are indicated by cyan boxes where the three-dimensional structure has been determined by NMR or X-ray crystallography. The core conserved amino acids are highlighted in orange boxes (Feinstein *et al.*, 1995). Residues at the homodimer or heterodimer interface observed structurally (Xiao *et al.*, 1999) or suggested by mutagenesis (Martin *et al.*, 1999; Jeong *et al.*, 1999; Bang *et al.*, 2000; Hill *et al.*, 2004; Berglund *et al.*, 2000; Huang *et al.*, 1996; Vaishnaw *et al.*, 1999; Straus *et al.*, 2001; Telliez *et al.*, 2000) are coloured red.

are essentially the same and consist of six antiparallel helices (Fig. 3), as also found for the other members of the death-domain superfamily (Weber & Vincenz, 2001; Kohl & Grutter, 2004). A well ordered 3_{10}-helix precedes α3 (Figs. 2 and 4). The loop between α1 and α2 forms a 3_{10}-helix in monomers *A* and *B* but only a turn in monomers *C*, *D*, *E* and *F*. The loop between α4 and α5 is flexible, as indicated by its *B* factors (Fig. 5). In comparison with the other helices, α6 is more mobile, as indicated by its *B* factors and the structural deviations when the six monomers are superimposed (Fig. 5).

3.2. Comparison with other structures

A search of the PDB with the program *DALI* (Holm & Sander, 1997) revealed that the three structures most similar to the UNC5H2 DD were those of the p75 neurotrophin DD (PDB code 1ngr, *DALI Z* score = 7.5, r.m.s.d. = 3.0 Å over 77 C^{α} residues; Liepinsh *et al.*, 1997), the apoptotic protease activating factor 1 (Apaf-1) CARD (PDB code 1cy5, chain *A*, *DALI Z* score = 7.3, r.m.s.d. = 2.6 Å over 74 C^{α} residues; Vaughn *et al.*, 1999) and the Pelle DD (PDB code 1d2z, chain *A*, *DALI Z* score = 7.0, r.m.s.d. = 2.5 Å over 73 C^{α} residues; Xiao *et al.*, 1999). Their sequence identities are 25, 7 and 18%, respectively. The proteins with the next highest similarities are the mucosa-associated lymphoid tissue lymphoma translocation protein 1 (MALT-1) DD (PDB code 2g7r, chain *A*, *DALI Z* score = 6.4, r.m.s.d. = 2.3 Å over 63 C^{α} residues), the interleukin-1 receptor-associated kinase 4 (IRAK4) DD (PDB code 1wh4, chain *A*, *DALI Z* score = 6.3, r.m.s.d. = 2.7 Å over 72 C^{α} residues), the Iceberg CARD (PDB code 1dgn, *DALI Z* score = 5.9, r.m.s.d. = 3.0 Å over 72 C^{α} residues; Plaizier-Vercammen & De Neve, 1982), the procaspase-9 CARD (PDB code 3ygw, chain *P*, *DALI Z* score = 5.8, r.m.s.d. = 2.7 Å over 72 C^{α} residues; Qin *et al.*, 1999) and the TNFR-1 DD (PDB code 1ich, *DALI Z* score = 5.5, r.m.s.d. = 3.0 Å over 74 C^{α} residues; Sukits *et al.*, 2001; Choi & Benveniste, 2004). Their sequence identities are 22, 21, 15, 15 and 12%, respectively.

3.3. Protein–protein interface

In order to determine the predominant species in solution, the molecular weight of the UNC5H DD was measured by analytical ultracentrifugation. Both sedimentation-velocity and sedimentation-equilibrium experiments were carried out using UV absorption. The sedimentation-velocity data revealed that the UNC5H DD sedimented as a single species, with a molecular weight estimated as 20.6 kDa. Sedimentation equilibrium yielded a molecular-weight value of 20 310 Da. The expected molecular weight of the dimer is 22 010 Da. The fit of the data to a single ideal species model is shown in Fig. 6.

The six protein monomers in the asymmetric unit are arranged in an approximately linear array (Fig. 2). The interactions between the two monomers in the *A*–*B*, *C*–*D* and *E*–*F* pairs in the asymmetric unit are essentially the same and bury a total dimer surface area of 1215–1341 $Å^2$ (a monomer surface area of 607–670 $Å^2$), which represents 11.1–12.9% of the dimer surface area (11.0–13.3% of the monomer surface area). On the other hand, the interactions between the *B*–*C*, *D*–*E* and *F*–*A* pairs in the asymmetric unit are completely different from each other. Therefore, these *B*–*C*, *D*–*E* and *F*–*A* interfaces presumably do not reflect the biological contacts, although the buried areas are relatively large (1019–1248 $Å^2$, 10.8–11.5% of the dimer surface area). We conclude that the biological dimer interface is formed by *A*–*B*, *C*–*D* and *E*–*F*.

The monomer–monomer interactions of the dimer are formed by the 3_{10} and α3 helices in one monomer and the α4 helices in another monomer (Fig. 7) and are mainly hydro-

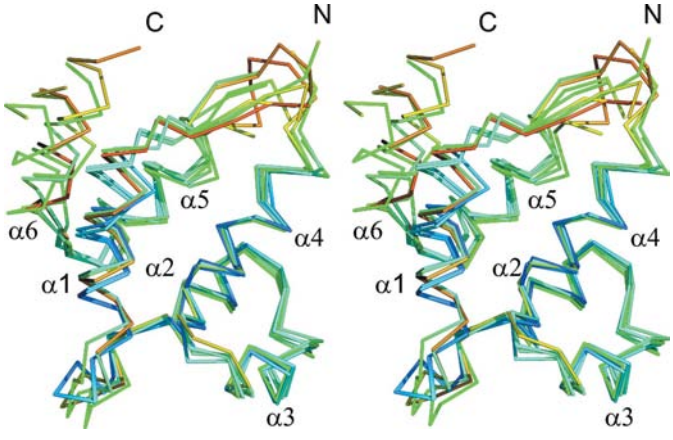

Figure 5
Stereoview showing a superposition of the C^{α} atoms of residues 858–912 and 921–938 in the six death domains in the crystallographic asymmetric unit. The protein chain is coloured according to the *B*-factor values, with lower values in green and higher values in orange. This figure was drawn using *PyMOL*.

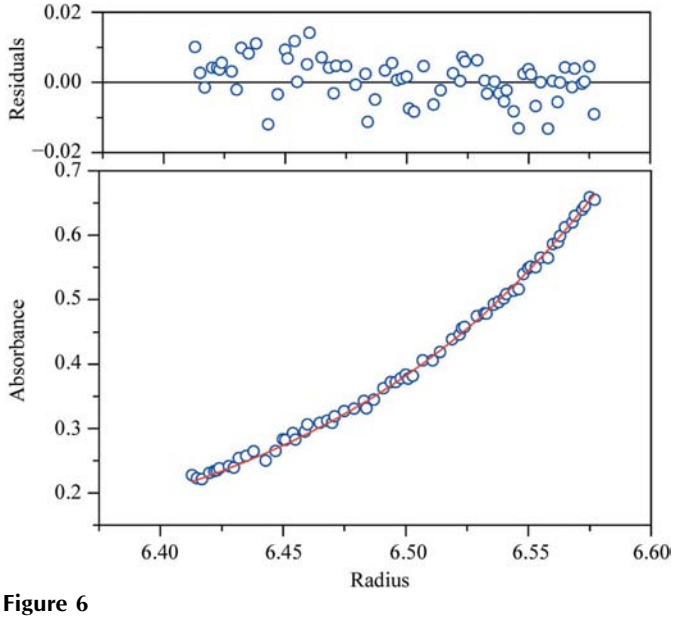

Figure 6
A plot of the sedimentation-equilibrium data with the residuals from the best fit to a single ideal species. This plot shows the data using 0.36 mg ml^{-1} of protein and a speed of 22 000 rev min^{-1}. The estimated partial specific volume of the protein is 0.724 ml g^{-1} and the solvent density was calculated to be 1.005 g ml^{-1}.

phobic and van der Waals interactions. The aliphatic side chain of Arg891 and the aromatic ring of Tyr892 in the 3_{10}-helix contact the side chain of Arg913 in α4, while the aromatic rings of Tyr892 in the 3_{10}-helix and Tyr895 in α3 interact with the side chain of Leu909 in α4 and the side chain of Tyr895 contacts the side chain of Ala912 in α4. In addition, Tyr895 O^{η} in α3 forms a water-mediated hydrogen bond with Asp908 O^{δ} in α4 (Figs. 4 and 7).

4. Discussion

The sequence alignment shows that the UNC5H2 DD is more similar to the p75 neurotrophin DD than to the death domains of IRAK4, Tube, Pelle, FADD, Fas and TNFR-1 (Fig. 4). These death domains are classified into two subtypes, subtypes 1 and 2, based on their sequence similarities. The p75 neurotrophin DD belongs to subtype 2 and the death domains of Tube, Pelle, FADD, Fas and TNFR-1 belong to subtype 1 (Feinstein *et al.*, 1995). In fact, the UNC5H2 DD has features that are characteristic of subtype 2: (i) there are conserved charged amino acids in α1, (ii) there is a shorter intervening region between α3 and α4 and (iii) two pairs of conserved proline residues are present in the regions between α1 and α2 and between α3 and α4. The *DALI* (Holm & Sander, 1997) search revealed that the three-dimensional structure of the UNC5H2 DD is also more similar to that of the p75 neurotrophin DD (Liepinsh *et al.*, 1997). In the crystal structure of the UNC5H2 DD, α2 and α4 are parallel to each other and the orientation of α3 is almost perpendicular to α2 and α4. The p75 neurotrophin DD, the Pelle DD, the TNFR-1 DD and the IRAK4 DD have the same relative orientations of α2, α3 and α4 as in the UNC5H2 DD (Liepinsh *et al.*, 1997; Xiao *et al.*, 1999; Sukits *et al.*, 2001; Lasker *et al.*, 2005). The p75 neurotrophin DD reportedly does not self-associate, as determined by its solution structure (Liepinsh *et al.*, 1997). Despite the similarities between the UNC5H2 DD and the p75 neurotrophin DD, the crystal structure of the UNC5H2 DD revealed dimer formation in the crystal, which was confirmed by the ultracentrifugation study. The residues involved in the self-association of the UNC5H2 DD are Arg891, Tyr892, Tyr895, Asp908, Leu909, Ala912 and Arg913, which are in the 3_{10}-helix and the α3 and α4 helices (Figs. 4 and 7). These amino-acid residues are not conserved in the p75 neurotrophin DD (Fig. 4).

In the death domains of Fas (Huang *et al.*, 1996) and FADD (Jeong *et al.*, 1999; Berglund *et al.*, 2000), the charged surface formed by α2 and α3 has been implicated in both homo and hetero associations (Fig. 4). In the TNFR-1 DD, a charged binding surface constituted by α2 and part of α3 and another binding surface formed by α4 have been implicated in homo and hetero associations (Sukits *et al.*, 2001). In the complex structure of the Tube and Pelle death domains, helices α4 and α5 of the Pelle DD interact with α6 and the long C-terminal tail of the Tube DD and their interactions involve a mixture of hydrogen bonds and van der Waals interactions (Xiao *et al.*, 1999). In the complex structure of the Apaf-1 and procaspase-9 CARDs, α1a/α1b and α4 of the Apaf-1 CARD interact with a convex surface formed by helices α2 and α3 of the procaspase-9 CARD by specific recognition mediated by hydrogen bonds and van der Waals interactions (Vaughn *et al.*, 1999). Death domains display considerable sequence diversity and have no conserved interaction surface, although their overall folds are very similar (Weber & Vincenz, 2001). Death domains may associate by a variety of mechanisms, according to their cellular and molecular functions. Our structure represents an example of the homodimeric interactions of death domains.

In the presence of netrin 1, UNC5H and DCC mediate axonal guidance (Fig. 1*a*). An interaction between the cytoplasmic domains of DCC and UNC5H is required for repulsion to netrin 1 (Fig. 1*a*). *In vitro Xenopus* assays have revealed that the association between the P1 domain of DCC and the DB domain of UNC5H mediates this repulsion (Hong *et al.*, 1999). *In vivo Drosophila melanogaster* assays showed that UNC5, the UNC5H homologue of *Drosophila*, elicits repulsion to netrin 1 in the absence of DCC (Keleman & Dickson, 2001; Fig. 1*a*). In this case, the death domain of UNC5 is strictly required for both the DCC-dependent and DCC-independent repulsions (Keleman & Dickson, 2001). The homodimerization of the mammalian UNC5H2 death domain may play an important role in the DCC-independent repulsion (Fig. 1*a*).

In the absence of netrin 1, UNC5H1–3 triggers apoptosis. The caspase cleavage of UNC5H2 is required for apoptosis induction (Llambi *et al.*, 2001; Tanikawa *et al.*, 2003; Fig. 1*b*). The death domain is located at the C-terminus of the caspase-cleavage site and is essential for apoptosis (Llambi *et al.*, 2001). UNC5H2-induced apoptosis is mediated by DAP-kinase, which interacts with the UNC5H2 DD (Llambi *et al.*, 2005). In the case of p75 neurotrophin, dimerization is essential for inhibiting its pro-apoptotic effect (Wang *et al.*, 2000). The apoptosis-

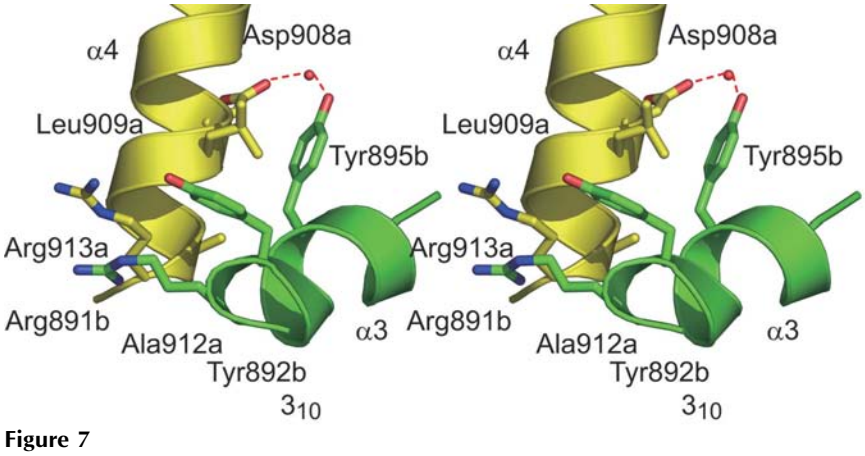

Figure 7
Detailed view of the dimer interfaces. Interacting residues are displayed as ball-and-stick models. Hydrogen bonds are indicated by red dots. The molecules are coloured as in Fig. 2. This figure was drawn using *PyMOL*.

inhibiting dimerization requires the carboxy-terminal 19 amino acids, which include α6 of the death domain and the carboxy-terminal nonhelical region (Wang *et al.*, 2000). These results suggest that the netrin 1 binding of UNC5H2 induces dimerization, thus blocking caspase cleavage (Arakawa, 2005) (Fig. 1*b*). In the crystal structure of the UNC5H2 DD, the total contact area of the dimer is relatively small. Thus, it is possible that netrin 1 is necessary for stabilization of the death-domain dimer. From this point of view, the apototic inductions of p75 neurotrophin and UNC5H2 are quite different from those of the Fas and TNFR-1 DDs. In Fas-induced apoptosis, the Fas DD is trimerized and then recruits FADD after binding the Fas ligand, leading to apoptosis (Siegel *et al.*, 2000; Choi & Benveniste, 2004). TNFR-1 DD trimerization upon binding to the TNF trimer recruits the TNFR-associated death-domain protein (TRADD) and then triggers the formation of a TNFR-1-induced apoptosis signalling complex (Smith *et al.*, 1994; Hsu *et al.*, 1995). The multimerization of DCC is mediated by the self-association of the P3 domains (Stein *et al.*, 2001). Our results suggest that the multimerization of UNC5H2 is mediated, at least in part, by the death domain. In contrast to p75 neurotrophin, the dimer interaction is formed by α3, α4 and the 3_{10}-helix preceding α3 of the death domain in UNC5H2.

We thank Dr Masaki Yamamoto for help in data collection at the RIKEN beamline BL26B1 of SPring-8. We thank Mr Satoshi Morita, Ms Yukiko Kinoshita, Mr Hiroaki Hamana, Ms Yuki Kamewari, Ms Hiroko Uda-Tochio, Ms Yuri Tomabechi and Ms Keiko Nagano for purification of the proteins. We also thank Ms Yumiko Fujikura, Ms Natsuko Matsuda, Ms Yoko Motoda, Ms Miyuki Saito, Ms Yukako Miyata, Mr Atsuo Kobayashi, Ms Noriko Hirakawa, Ms Noriko Sakagami, Mr Masaomi Ikari, Ms Fumiko Hiroyasu, Ms Yasuko Tomo and Ms Megumi Watanabe for their technical assistance in sample preparations. We thank Dr Satoru Unzai for help in the analysis of the analytical ultracentrifugation data. This work was supported by the RIKEN Structural Genomics/Proteomics Initiative (RSGI), the National Project on Protein Structural and Functional Analyses, Ministry of Education, Culture, Sports, Science and Technology of Japan.

References

Arakawa, H. (2004). *Nature Rev. Cancer*, **4**, 978–987.

Arakawa, H. (2005). *Cell Death Differ.* **12**, 1057–1065.

Bang, S., Jeong, E. J., Kim, I. K., Jung, Y. K. & Kim, K. S. (2000). *J. Biol. Chem.* **275**, 36217–36222.

Berglund, H., Olerenshaw, D., Sankar, A., Federwisch, M., McDonald, N. Q. & Driscoll, P. C. (2000). *J. Mol. Biol.* **302**, 171–188.

Bredesen, D. E., Mehlen, P. & Rabizadeh, S. (2004). *Physiol. Rev.* **84**, 411–430.

Brünger, A. T., Adams, P. D., Clore, G. M., DeLano, W. L., Gros, P., Grosse-Kunstleve, R. W., Jiang, J.-S., Kuszewski, J., Nilges, M., Pannu, N. S., Read, R. J., Rice, L. M., Simonson, T. & Warren, G. L. (1998). *Acta Cryst.* D**54**, 905–921.

Carninci, P. *et al.* (2003). *Genome Res.* **13**, 1273–1289.

Carrington, P. E., Sandu, C., Wei, Y., Hill, J. M., Morisawa, G., Huang, T., Gavathiotis, E., Wei, Y. & Werner, M. H. (2006). *Mol. Cell*, **22**, 599–610.

Choi, C. & Benveniste, E. N. (2004). *Brain Res. Brain Res. Rev.* **44**, 65–81.

Feinstein, E., Kimchi, A., Wallach, D., Boldin, M. & Varfolomeev, E. (1995). *Trends Biochem. Sci.* **20**, 342–344.

Hill, J. M., Morisawa, G., Kim, T., Huang, T., Wei, Y., Wei, Y. & Werner, M. H. (2004). *J. Biol. Chem.* **279**, 1474–1481.

Hofmann, K. & Tschopp, J. (1995). *FEBS Lett.* **371**, 321–323.

Holm, L. & Sander, C. (1997). *Nucleic Acids Res.* **25**, 231–234.

Hong, K., Hinck, L., Nishiyama, M., Poo, M. M., Tessier-Lavigne, M. & Stein, E. (1999). *Cell*, **97**, 927–941.

Hsu, H., Xiong, J. & Goeddel, D. V. (1995). *Cell*, **81**, 495–504.

Huang, B., Eberstadt, M., Olejniczak, E. T., Meadows, R. P. & Fesik, S. W. (1996). *Nature (London)*, **384**, 638–641.

Jeong, E. J., Bang, S., Lee, T. H., Park, Y. I., Sim, W. S. & Kim, K. S. (1999). *J. Biol. Chem.* **274**, 16337–16342.

Keino-Masu, K., Masu, M., Hinck, L., Leonardo, E. D., Chan, S. S., Culotti, J. G. & Tessier-Lavigne, M. (1996). *Cell*, **87**, 175–185.

Keleman, K. & Dickson, B. J. (2001). *Neuron*, **32**, 605–617.

Kigawa, T., Yabuki, T., Matsuda, N., Matsuda, T., Nakajima, R., Tanaka, A. & Yokoyama, S. (2004). *J. Struct. Funct. Genomics*, **5**, 63–68.

Kigawa, T., Yabuki, T. & Yokoyama, S. (1999). *Tanpakushitsu Kakusan Koso*, **44**, 598–605.

Kigawa, T., Yabuki, T., Yoshida, Y., Tsutsui, M., Ito, Y., Shibata, T. & Yokoyama, S. (1999). *FEBS Lett.* **442**, 15–19.

Kohl, A. & Grutter, M. G. (2004). *C. R. Biol.* **327**, 1077–1086.

Koradi, R., Billeter, M. & Wuthrich, K. (1996). *J. Mol. Graph.* **14**, 51–55.

Kraulis, P. J. (1991). *J. Appl. Cryst.* **24**, 946–950.

Lasker, M. V., Gajjar, M. M. & Nair, S. K. (2005). *J. Immunol.* **175**, 4175–4179.

Laskowski, R. A., Rullmannn, J. A., MacArthur, M. W., Kaptein, R. & Thornton, J. M. (1996). *J. Biomol. NMR*, **8**, 477–486.

Laue, T. M., Shah, B., Ridgeway, T. M. & Pelletier, S. L. (1992). *Analytical Ultracentrifugation in Biochemistry and Polymer Science*, edited by S. E. Harding, A. D. Rowe & J. C. Horton, pp. 90–125. Cambridge: Royal Society of Chemistry.

Leonardo, E. D., Hinck, L., Masu, M., Keino-Masu, K., Ackerman, S. L. & Tessier-Lavigne, M. (1997). *Nature (London)*, **386**, 833–838.

Liepinsh, E., Ilag, L. L., Otting, G. & Ibanez, C. F. (1997). *EMBO J.* **16**, 4999–5005.

Llambi, F., Causeret, F., Bloch-Gallego, E. & Mehlen, P. (2001). *EMBO J.* **20**, 2715–2722.

Llambi, F., Laurenco, F. C., Gozuacik, D., Guix, C., Pays, L., Del Rio, G., Kimchi, A. & Mehlen, P. (2005). *EMBO J.* **24**, 1192–1201.

Martin, D. A., Zheng, L., Siegel, R. M., Huang, B., Fisher, G. H., Wang, J., Jackson, C. E., Puck, J. M., Dale, J., Straus, S. E., Peter, M. E., Krammer, P. H., Fesik, S. & Lenardo, M. J. (1999). *Proc. Natl Acad. Sci. USA*, **96**, 4552–4557.

Mazelin, L., Bernet, A., Bonod-Bidaud, C., Pays, L., Arnaud, S., Gespach, C., Bredesen, D. E., Scoazec, J. Y. & Mehlen, P. (2004). *Nature (London)*, **431**, 80–84.

Mehlen, P. & Furne, C. (2005). *Cell. Mol. Life Sci.* **62**, 2599–2616.

Mehlen, P. & Mazelin, L. (2003). *Biol. Cell*, **95**, 425–436.

Mehlen, P., Rabizadeh, S., Snipas, S. J., Assa-Munt, N., Salvesen, G. S. & Bredesen, D. E. (1998). *Nature (London)*, **395**, 801–804.

Merritt, E. A. & Murphy, M. E. (1994). *Acta Cryst.* D**50**, 869–873.

Otwinowski, Z. & Minor, W. (1997). *Methods Enzymol.* **276**, 307–326.

Park, H. H. & Wu, H. (2006). *J. Mol. Biol.* **357**, 358–364.

Plaizier-Vercammen, J. A. & De Neve, R. E. (1982). *J. Pharm. Sci.* **71**, 552–556.

Qin, H., Srinivasula, S. M., Wu, G., Fernandes-Alnemri, T., Alnemri, E. S. & Shi, Y. (1999). *Nature (London)*, **399**, 549–557.

Schuck, P. (1998). *Biophys. J.* **75**, 1503–1512.

Siegel, R. M., Frederiksen, J. K., Zacharias, D. A., Chan, F. K., Johnson, M., Lynch, D., Tsien, R. Y. & Lenardo, M. J. (2000). *Science*, **288**, 2354–2357.
Smith, C. A., Farrah, T. & Goodwin, R. G. (1994). *Cell*, **76**, 959–962.
Stein, E., Zou, Y., Poo, M. & Tessier-Lavigne, M. (2001). *Science*, **291**, 1976–1982.
Straus, S. E. *et al.* (2001). *Blood*, **98**, 194–200.
Sukits, S. F., Lin, L. L., Hsu, S., Malakian, K., Powers, R. & Xu, G. Y. (2001). *J. Mol. Biol.* **310**, 895–906.
Tanikawa, C., Matsuda, K., Fukuda, S., Nakamura, Y. & Arakawa, H. (2003). *Nature Cell Biol.* **5**, 216–223.
Telliez, J. B., Xu, G. Y., Woronicz, J. D., Hsu, S., Wu, J. L., Lin, L., Sukits, S. F., Powers, R. & Lin, L. L. (2000). *J. Mol. Biol.* **300**, 1323–1333.
Terwilliger, T. (2004). *J. Synchrotron Rad.* **11**, 49–52.
Terwilliger, T. C. & Berendzen, J. (1999). *Acta Cryst.* D**55**, 849–861.
Thiebault, K., Mazelin, L., Pays, L., Llambi, F., Joly, M. O., Scoazec, J. Y., Saurin, J. C., Romeo, G. & Mehlen, P. (2003). *Proc. Natl Acad. Sci. USA*, **100**, 4173–4178.
Vaishnaw, A. K., Orlinick, J. R., Chu, J. L., Krammer, P. H., Chao, M. V. & Elkon, K. B. (1999). *J. Clin. Invest.* **103**, 355–363.
Vaughn, D. E., Rodriguez, J., Lazebnik, Y. & Joshua-Tor, L. (1999). *J. Mol. Biol.* **293**, 439–447.
Wada, T., Shirouzu, M., Terada, T., Ishizuka, Y., Matsuda, T., Kigawa, T., Kuramitsu, S., Park, S. Y., Tame, J. R. & Yokoyama, S. (2003). *Acta Cryst.* D**59**, 1213–1218.
Wang, J. J., Rabizadeh, S., Tasinato, A., Sperandio, S., Ye, X., Green, M., Assa-Munt, N., Spencer, D. & Bredesen, D. E. (2000). *J. Neurosci. Res.* **60**, 587–593.
Weber, C. H. & Vincenz, C. (2001). *Trends Biochem. Sci.* **26**, 475–481.
Xiao, T., Towb, P., Wasserman, S. A. & Sprang, S. R. (1999). *Cell*, **99**, 545–555.